Nanochem. Res., 8(4): 287-298, Autumn 2023

RESEARCH PAPER

Aqueous Synthesis of Sub-11 nm Fe-Cu Oxides and Alloy Nanostructures: Structural and Morphological Studies

Raquel Zúñiga-Lechuga[1], Alfredo R. Vilchis-Nestor[2]*, Raúl A. Morales-Luckie[2], Victor Sánchez-Mendieta[1,2]†

[1]Posgrado en Ciencia de Materiales. Facultad de Química, Universidad Autónoma del Estado de México Paseo Colón y Paseo Tollocan. Toluca, Estado de México. 50120. México
[2]Centro Conjunto de Investigación en Química Sustentable UAEM-UNAM, Carretera Toluca-Ixtlahuaca Km 14.5, San Cayetano, Toluca, Estado de México, 50200. México

ARTICLE INFO

Article History:
Received 06 Jul 2023
Accepted 17 Sep 2023
Published 01 Oct 2023

Keywords:
Iron-copper oxides,
Iron-copper nanoalloy,
Electron microscopy,
X-Ray Photoelectron Spectroscopy.

ABSTRACT

Fe and Cu oxides and Fe-Cu alloy nanostructures (FeCuNS) were obtained using a facile chemical reduction of different mass ratios of $FeCl_2 \cdot 4H_2O$ and $CuCl_2 \cdot 2H_2O$ with $NaBH_4$ in an aqueous solution, under nitrogen atmosphere. FeCuNS were prepared in three different Fe:Cu ratios: 75:25, 50:50, and 25:75 wt. %, by an aqueous reduction. FeCuNS were characterized by Scanning Electron Microscopy (SEM), X-Ray Photoelectron Spectroscopy (XPS), X-Ray Diffraction (XRD), Transmission Electron Microscopy (TEM), and High-Resolution TEM (HRTEM), and their textural properties were determined using nitrogen physisorption. Synthesized FeCuNS sizes ranged from 2.2 to 11 nm, having an irregular quasi-spherical morphology. The main phases in these nanostructures, as determined by XRD, are Fe_2O_3, Fe_3O_4 and $CuFe_2O_4$; the main peak obtained at $2\theta = 43.33°$ confirmed the formation of the nanoalloy Fe-Cu, as $FeCu_4$ (JCPDS No.065-7002) in the 50:50 and 25:75 wt.% FeCuNS samples, which can be indexed as a face-centered cubic structure (FCC). An XPS study performed on these nanostructures allowed for confirming the formation of the $FeCu_4$ alloy, alongside other metallic oxide main phases.

How to cite this article
Zúñiga-Lechuga R., Vilchis-Nestor A. R., Morales-Luckie R. A., Sánchez-Mendieta V., Aqueous synthesis of sub-11 nm Fe-Cu oxides and alloy nanostructures: structural and morphological studies. Nanochem. Res., 2023; 8(4): 287-298. DOI: 10.22036/NCR.2023.04.07

INTRODUCTION

Bimetallic nanoparticles have demonstrated to possess better properties than monometallic nanoparticles mainly due to the additive properties of the two metal components. Iron and copper oxides nanoparticles have been synthesized for several years, and their interesting properties and applications have been reported. Magnetite (Fe_3O_4), hematite (α-Fe_2O_3), and maghemite (γ-Fe_2O_3) are magnetic materials which have been applied as nanomaterials in areas such as catalysis, biomedicine, data storage devices, magnetic fluids, gas sensors, magnetic resonance imaging, among others [1,2]. Copper and copper oxides nanoparticles are recognized for their high electrical conductivity, with potential applications in fields including electronics, optics, and catalysis [3,4]. Thus, the combination of Fe and Cu and/or their oxides in a nanostructure can provide very interesting properties that widens the potential applications for that functional nanomaterial. For instance, bimetallic copper-iron oxide nanoparticles have been synthesized throughout a simple chemical precipitation methodology; and

* Corresponding Author Email: *arvilchisn@uaemex.mx*
† Corresponding Author Email: *vsanchezm@uaemex.mx*

these bimetallic nanoparticles have been employed to add electrical and magnetic properties to leather for lighting applications [5]. Furthermore, bimetallic iron-copper oxide nanoparticles supported on nanometric diamond have been employed as an efficient and stable sunlight-assisted Fenton photocatalyst [6]. Additionally, Fe-Cu oxides nanostructures were obtained using Virginia Creeper (*Parthenocissus quinquefolia*) leaf extract in the presence of oxalic acid; these nanomaterials were used for the removal of green malachite from water [7]. Moreover, nanoalloys have drawn increasing research interest owing to their structural studies [8-12] and their potential applications in catalysis [13-15], surface plasma band energy [16,17], optoelectronics, information storage, adsorption process, magnetic properties [18,19], among others. The study of transition metal clusters and metallic alloys has been also developed both theoretically and experimentally, with great interest in their applications for the removal of contaminants [11,14,15]. These kinds of applications are closely related to the *sui generis* properties of each metal forming the alloy and determined, also, by their shape, size distribution and composition [20]. The growing interest in Fe-Cu nanoalloy has risen due to its bulk immiscibility, the intrinsic magnetic properties, and the synergistic effects of two-metal redox couples between iron and copper [21-24]. This nanoalloy has been used in electronic, chemical, and environmental research [25], due to their magnetic and catalytic properties. Individually, iron nanoparticles have many attractive applications [26] mainly in optics [27], magnetism [28], electrical devices [29], electrocatalysis [30], and environmental remediation [31]. Likewise, copper nanoparticles have been used in optical [32], magnetic [33] and sensor devices [34], catalysis [35] and environmental remediation [36] as well as antifungal and bacteriostatic agents [37]. Several methods have been applied for the preparation of bimetallic nanoparticles, including alcohol reduction [13], citrate reduction [17,38], polyol processes [39], borohydride reduction [40], solvent extraction–reduction [16,41,42], sonochemical methods [43], photolytic reduction [44,45], radiolytic reduction [46,47], laser ablation [48,49], and biological programming [50]. Mechanical alloying, using the high energy ball milling (BM), was also proved to be useful for synthesizing various phases [13,14,20]. Thus, chemical reduction methods have confirmed to be relatively simple and useful when small size nanoparticles are required for catalytic applications; these particles usually have 10 to 1000 times greater reactivity compared with particles obtained by other methods [51].

In this work, a series of FeCuNS were prepared by an aqueous chemical reduction methodology, utilizing sodium borohydride as a reducing agent and iron and copper chlorides as metal precursors. The FeCuNS were thoroughly analyzed by XRD, SEM, EDS, TEM and XPS to obtain their chemical, structural and morphological characteristics.

EXPERIMENTAL

Materials and Methods

All chemical reagents were of analytical grade, commercially acquired, and used without further purification. All solutions were prepared with deionized water (with ρ 18.2 MΩ cm) obtained from a Mili-Q System (Millipore, USA).

In a typical preparation of FeCuNS, 1 M $FeCl_2{\cdot}4H_2O$ (Fermont) and 1 M $CuCl_2{\cdot}2H_2O$ (J.T. Baker) aqueous solutions were combined in a 1:1 ratio. The mixture was stirred vigorously for one hour, followed by reduction using a 4 M $NaBH_4$ aqueous solution (98%, Aldrich). Nitrogen gas was bubbled during synthesis to evacuate oxygen and to prevent the complete oxidation of Fe-Cu nanoparticles. A fine black precipitate was obtained, which was filtrated and washed two times with deionized water. Further syntheses of the nanoalloy were performed with three different Fe:Cu mass ratios (75:25, 50:50, 25:75 wt.% FeCuNS, respectively), following the same reaction conditions described above. The crystalline phases of the Fe-Cu samples were identified by X-ray diffraction (XRD) patterns, which were collected on a Bruker D8 Advance powder diffraction system using Cu-Kα radiation (λ = 0.15406 nm) in 2θ range from 5 to 70°, operating at 35 kV and 35 mA, with the scanning speed of 0.02° s^{-1}. X-ray photoelectron spectra (XPS) for all samples were collected using a JEOL JPS-9200, equipped with a Mg X-ray source (1253.6 eV) at 200 W over an analysis area of 1 mm^2 under vacuum on the order of 1×10^{-8} Torr. Survey and narrow spectra were recorded and scannedwith an energy pass of 50 and 20 eV, respectively. The spectra were analyzed using the Specsurf™ software included with the instrument. The surface chemical composition was determined from the corresponding peak area. Corrections of charging of the scanned elements

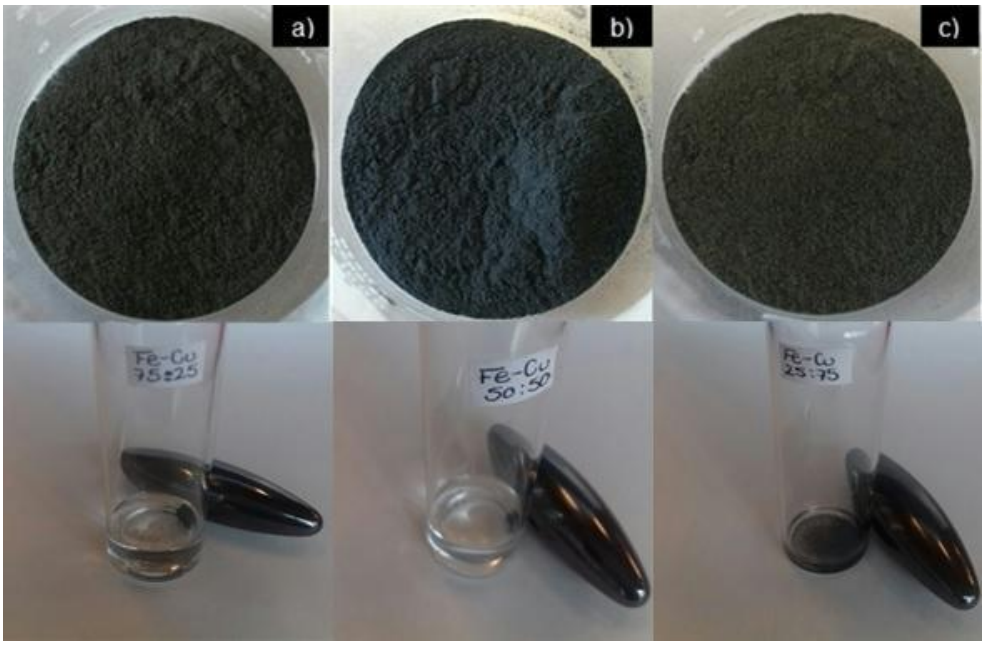

Fig. 1 Photographs of the blackish precipitate obtained from different metal concentration ratios (top) and corresponding FeCuNS dispersed in water and attracted by a magnet (bottom): a) Fe:Cu 75:25 wt.%, b) Fe:Cu 50:50 wt.% and c) Fe:Cu 25:75 wt.%

were carried out taking the carbon signal (C1s) at 284.5 eV as the reference point. The Shirley method was used for the background subtraction, whereas curve fitting was conducted with the Gauss-Lorentz method. SEM observations were carried out on a JEOL JSM-6510LV operated at 20 kV accelerating voltage. Each FeCuNS sample was attached to aluminum stub using conductive double-stick carbon tape and observed without coating. Elemental characterization was performed using an OXFORD Energy-Dispersive X-Ray spectroscope with a resolution of 137 eV anchored to the Scanning Electron Microscope. A FEG Hitachi S-5500 ultra-high-resolution electron microscope (0.4 nm at 15 kV) with a BF/DF Duo STEM detector attached to an EDS-probe (from Bruker) was employed. Transmission electron microscopy (TEM) micrographs and SAED patterns were collected in a JEOL JEM-2100 microscope operated at 200 kV with LaB_6 filament. Samples were prepared in the following way: each FeCuNS was dispersed in isopropyl alcohol, and then one drop of this suspension was placed in a copper grid coated with carbon. Finally, the grid was allowed to air-dry. Brunauer–Emmett–Teller (BET) surface areas were determined by standard multipoint techniques of nitrogen adsorption, using an Autosorb iQ Station 1 of Quantachrome Instruments. Samples were heated at 200°C for 2 h, before measuring the specific surface areas.

RESULTS AND DISCUSSION

The chemical reduction of $FeCl_2{\cdot}4H_2O$ and $CuCl_2{\cdot}2H_2O$ aqueous solutions, using $NaBH_4$ as a reducing agent, yielded a black fine precipitate. Fig. 1 shows pictures of the precipitate, with the characteristic blackened color of iron oxides. Additionally, a magnetic response of the powder can be seen when a magnet approaches the glass vial. This behavior was more obvious, as expected, in the FeCuNS samples with 75:25 and 50:50 wt%.

XRD patterns of the as-prepared FeCuNS (75:25, 50:50 and 25:75 wt. %) are shown in Fig. 2. Three different phases of FeCuNS: Cu_xFe_{1-x}, $CuFe_2O_4$, and $FeCu_4$ can be detected in the samples and confirmed by the cards JCPDS 49-1399, 25-0283 and 65-7002, respectively. The peak obtained at $2\theta = 43.33°$ shows the formation of the Fe-Cu nanoalloy (JCPDS No.065-7002 like $FeCu_4$) in the 50:50 wt.% and 25:75 wt.% samples, respectively, which can be indexed on the basis of a face–centered cubic structure (FCC) [52]. Figs. 2b-c show diffraction peaks at $2\theta = 35°$, which can be associated to copper ferrite ($CuFe_2O_4$) and are assigned to the (103) plane. In addition, the 75:25 wt. % sample (Fig. 2a) illustrates the peak at $2\theta = 30.1°$. The presence of $CuFe_2O_4$ (JCPDS No.25-0283) diffraction peaks is evidence of the strong bimetallic interaction, which

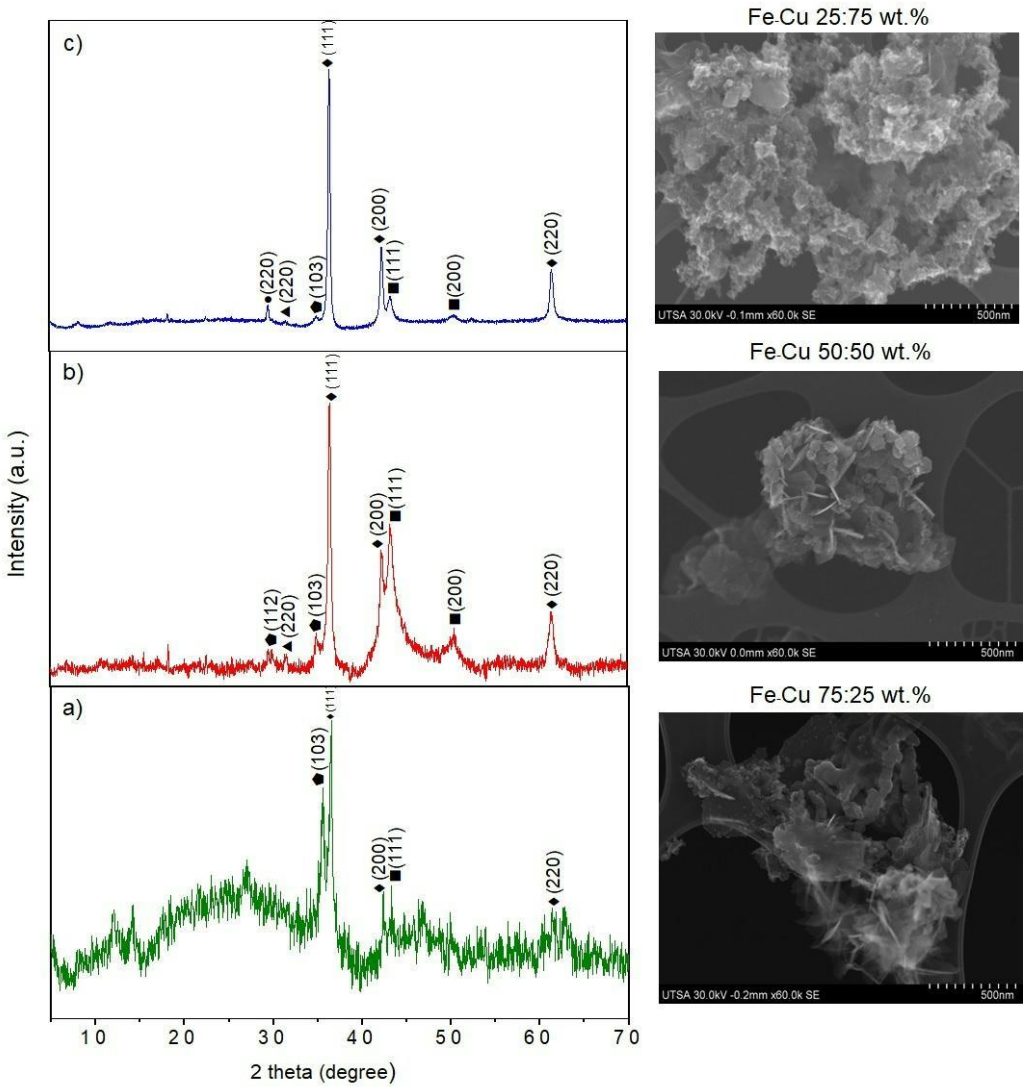

Fig. 2 XRD pattern of the FeCuNS prepared at different concentration: a) Fe:Cu 75:25 wt.%, b) Fe:Cu 50:50 wt.% and c) Fe:Cu 25:75 wt.%. ● JCPDS No.49-1399 Cu_xFe_{1-x}, ⬟ JCPDS No.025-0283 $CuFe_2O_4$, ■ JCPDS No.065-7002 $FeCu_4$, ▲ JCPDS No.040-1139 Fe_2O_3, and ♦ JCPDS No.065-3288 Cu_2O

can lead to the formation of a spinel structure at nanoalloys. XRD analysis indicates that initial CuO was reduced to Cu_2O/Cu^0 in all the samples. The main peak of cuprite (Cu_2O) is oriented at (111), showing at 2θ = 36.43°, 35.45° and 36.53° for the 25:75 wt. %, 50:50 wt. % and 75:25 wt. % samples, respectively, as well as at 2θ = 42.32° in the 25:75 wt. % and 50:50 wt. % samples, oriented at (200); these peaks are in accordance with the reported values by [52]. The Fe-Cu nanoalloy showed distinct peaks at around 2θ = 43.30 and 50.5 (Figs. 2b-c), which could be attributed to Cu (JCPDS No.04-0836) or $FeCu_4$ (JCPDS No.65-7002). Since Cu and $FeCu_4$ have similar peaks in XRD patterns, it is hard to distinguish between these two phases. According to these results, it was found that there is an interaction between iron and copper oxides, promoting the dispersion of both species. In all samples, the absence of metallic copper or cuprous oxide signals suggested that either they are well dispersed or their peaks are overlapped with that coming from Fe_2O_3 at 2θ = 35.6°. In addition, a broadening of the diffraction peaks occurs gradually with increasing the mass concentration of Fe [52].

The elemental content of the superficial layers of the FeCuNS was obtained by XPS. The survey spectra, scanned from 0 to 1100 eV binding energy (BE), are shown in Fig. 3. To further confirm the

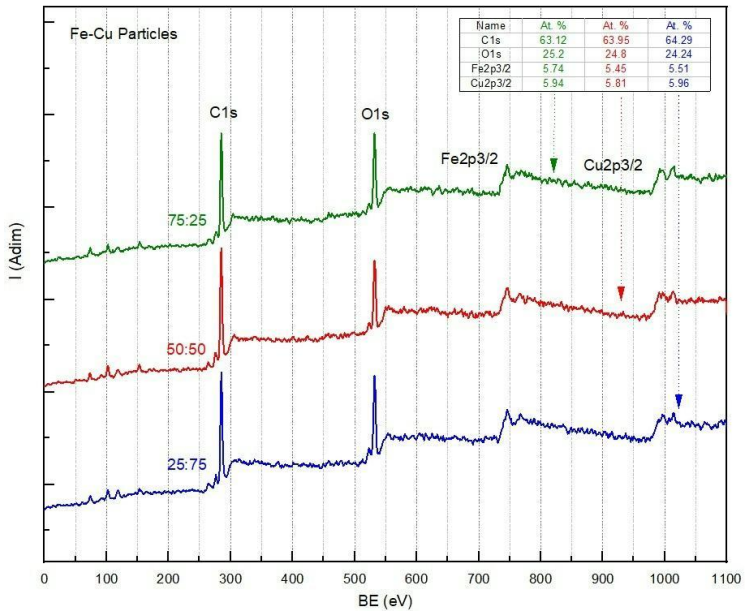

Fig. 3 XPS survey scans of the FeCuNS: a) Fe:Cu 75:25 wt.%, b) Fe:Cu 50:50 wt.% and c) Fe:Cu 25:75 wt.%

Table 1 EDS elemental analysis of FeCuNS.

Element	75:25 wt.% FeCuNS	50:50 wt.% FeCuNS	25:75 wt.% FeCuNS
C	12.09±3.77	16.13 ±1.24	13.97±2.30
O	11.26±1.15	31.6±3.61	28.67±1.51
Fe	54.47±1.72	26.42±2.90	24.96±2.33
Cu	22.16±2.73	25.78±3.00	32.00±2.13

existence of the Fe-Cu nanoalloy in the nanoparticles obtained, iron and copper elements were analyzed by deconvolution of their high resolution XPS spectra. In the three FeCuNS samples (Fig. 4), the different peaks observed correspond to different iron (FeO_2; Fe(OH)O; Fe_2O_3; Fe_3O_4) or iron-copper ($FeCuO_2$) oxide species. Only in the 25:75 wt.% FeCuNS sample, there is a peak at 706.7 eV, which can be attributed to the binding energy of the Fe-Cu nanoalloy (Fe $2p_{3/2}$). These results indicate that the Fe and Cu particles form a layer of diverse iron and copper oxides, which is due to the easily oxidizing zero-valent metals when exposed to air [51-53]. Furthermore, the presence of $FeCu_4$, showed by XRD, was confirmed by the signal at 706.7 eV, which can be assigned to Fe-Cu in the 25:75 wt.% FeCuNS sample. The presence of $FeCuO_2$ at 713.6 eV and from 714.1 to 716.9 eV in the 75:25 wt.% and 50:50 wt.% FeCuNS samples, respectively (Figs. 4a and b), confirms the presence of $CuFe_2O_4$, as obtained by XRD studies.

XPS spectra of Cu $2p_{3/2}$ are shown in Fig. 5. Two main photoelectron peaks at 932 to 932.9 eV can be observed in the 75:25 wt.%, 50:50 wt.% and 25:75 wt.% FeCuNS samples [54]; the peak at 932 eV confirmed that CuO was reduced to Cu_2O and metallic copper in all samples. O1s energetic distributions were adjusted with three Gaussian curves with FWHM = 1.4 ± 0.1 eV, as can be seen in Fig. 6. Regarding Fe $2p_{3/2}$ and Cu $2p_{3/2}$, each curve was assigned to a state or combination of states, according to its binding energy. The signal at 529.8 eV in Fig. 5c corresponds to $CuFe_2O_4$. Other peaks can be correlated to the different iron and copper oxides: Fe_2O_3, Cu_2O [55], in the 50:50 wt.% FeCuNS (Fig. 6b), and the iron oxides Fe_3O_4 and Fe_2O_3 in the 75:25 wt.% FeCuNS sample (Fig. 6a).

The morphology of the FeCuNS was analyzed by SEM. Fig. 7 shows the images of the 75:25 wt. %, 50:50 wt. % and 25:75 wt. % FeCuNS (Figs. 1a, b and c, respectively), where it is observed that the nanomaterials form agglomerates having rough surfaces [56]. EDS spectra were collected in two different regions of interest with a magnification of 2,000x for each FeCuNS. The results of chemical analysis by EDS are shown in Table 1, where similar

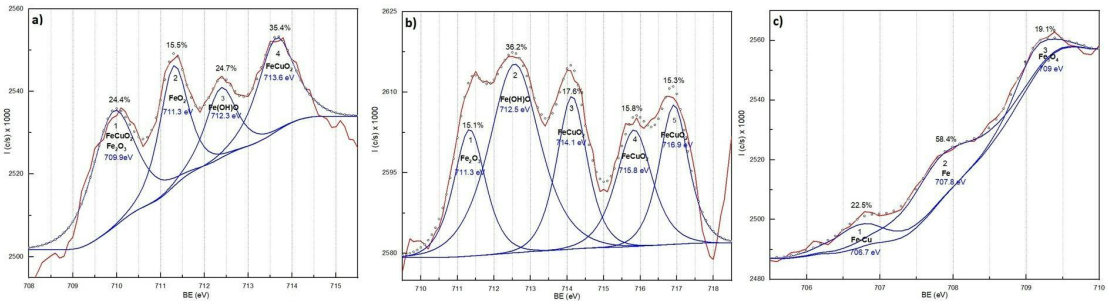

Fig. 4 XPS spectra of Fe $2p_{3/2}$ in the FeCuNS. a) Fe:Cu 75:25 wt.%, b) Fe:Cu 50:50 wt.% and c) Fe:Cu 25:75 wt.%

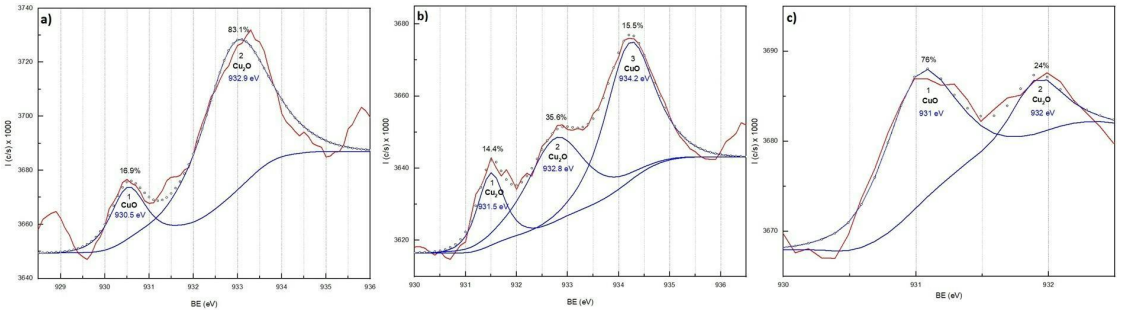

Fig. 5 XPS spectra of Cu $2p_{3/2}$ in the FeCuNS. a) Fe:Cu 75:25 wt.%, b) Fe:Cu 50:50 wt.% and c) Fe:Cu 25:75 wt.%

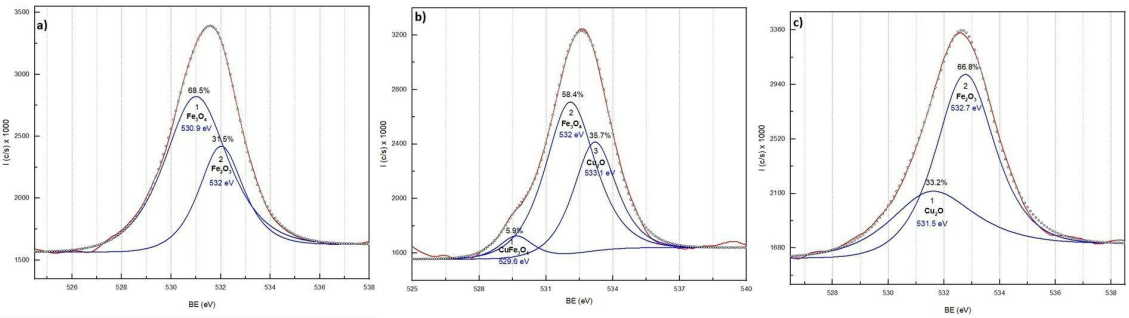

Fig. 6 XPS spectra of O1s in the FeCuNS. a) Fe:Cu 75:25 wt.%, b) Fe:Cu 50:50 wt.% and c) Fe:Cu 25:75 wt.%

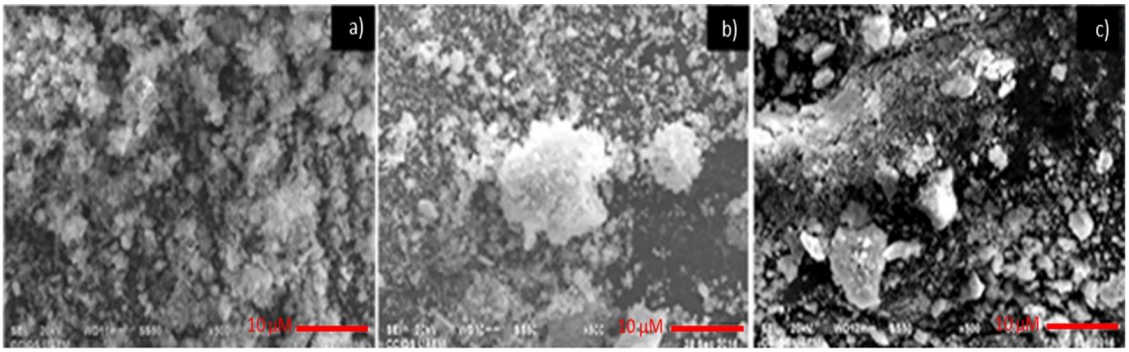

Fig. 7 SEM images of the FeCuNS. a) Fe:Cu 75:25 wt.%, b) Fe:Cu 50:50 wt.% and c) Fe:Cu 25:75 wt.% (scale bar = 10 μM)

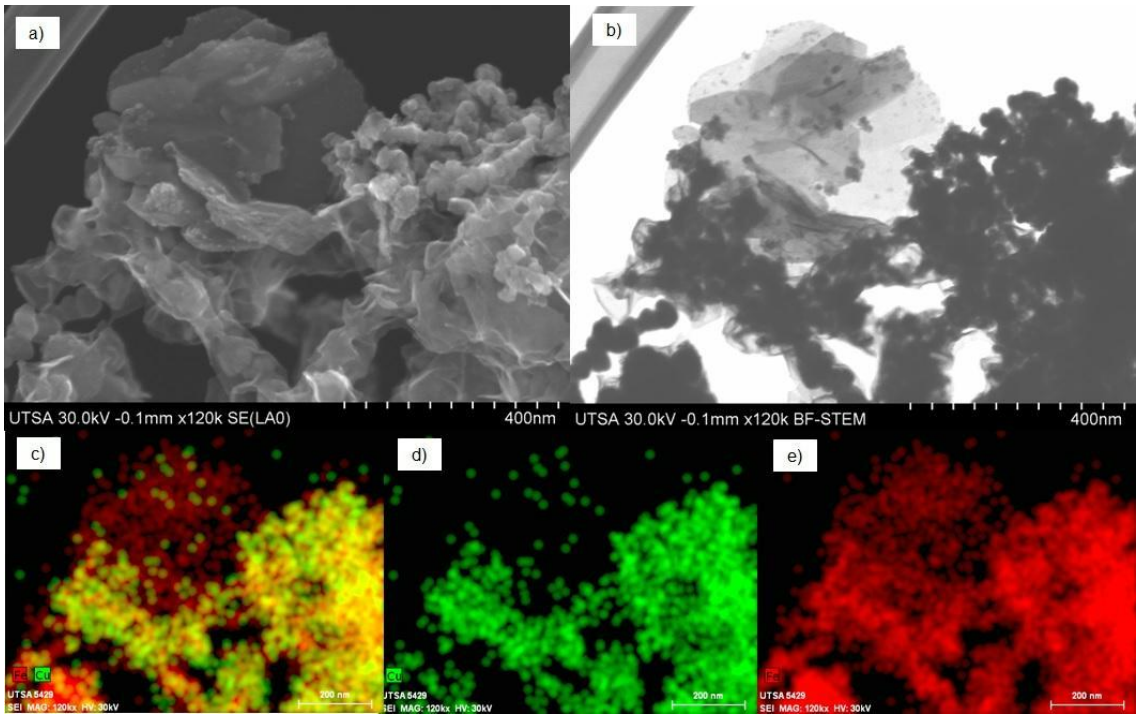

Fig. 8 a) FESEM image collected with secondary electron detector, b) STEM-DF image, c,d,e) EDS chemical mapping of Cu and Fe, respectively, of a sample of Fe:Cu 75:25 wt% FeCuNS.

proportions of 75:25, 50:50 and 25:75 wt.% FeCuNS were observed. Nevertheless, there is not an exact match between experimental and theoretical concentration of Fe and Cu due to the presence of oxygen associated with the formation of oxides during the synthesis.

The carbon content can be associated to the conducting C-tape, where the samples were mounted to perform the SEM-EDS analyses. Otherwise, the high oxygen content, observed in Table 1, can be explained due to the oxidation process of the bimetallic samples.

FESEM and STEM-BF images of the FeCuNS are shown in Figs. 8a and b, respectively. Their morphology can be described as irregular quasi-spheroidal particles with sizes smaller than 100 nm. EDS mapping (Figs. 8c-e) shows a homogeneous distribution of the Cu and Fe on the FeCuNS. From FESEM-BF image (Fig. 8b), it can be observed that the particles tend to mainly form agglomerates, but foil-like structures are also present.

It is known that different concentrations of the metal precursor solutions when forming the nanoalloy and the difference in the standard reduction potentials of Fe and Cu generate different bimetallic structures [9]. Moreover, there are reports of particles where Fe is at the center of the structure of the nanoalloy, forming the core of the particle, and Cu and Fe oxides are present too but in the shell [52]. Thus, the morphology of the obtained FeCuNS can be observed by a transmission electron microscopy (TEM) analysis. The images in Fig. 9 confirm the irregular quasi-spheroidal morphology of the FeCuNS. Size distribution histograms (depicted in the lower part of Fig. 9) of the FeCuNS were built from the measurement and analysis of 200 nanoparticles for each sample using representative TEM images. The particle size in the 75:25 wt.% FeCuNS sample shows the unimodal distribution of the synthesized nanostructures (Fig. 9a and bottom left of the histogram), with an average size of 7.7 nm (±3.4 nm). 50:50 wt. % and 25:75 wt. % FeCuNS samples demonstrate asymmetric distribution (Figs. 9b and c and bottom middle and right of the histograms, respectively), with an average size of 11 nm and (±5.5 nm) and 6.5 nm (±2.0 nm), respectively. HRTEM images (Fig. 10) show lattice spaces of 2.123 nm, 1.32 nm, and 1.035 nm between the (400), (531) and (553) planes, respectively, consistent with a Fe-Cu nanoalloy (JCPDF No.49-1399, as Cu_xFe_{1-x}). The HRTEM image in Fig. 10a reveals a fringe spacing of 1.887 nm in agreement with lattice spacing of the (331) plane of Fe_3O_4. The HRTEM micrograph in

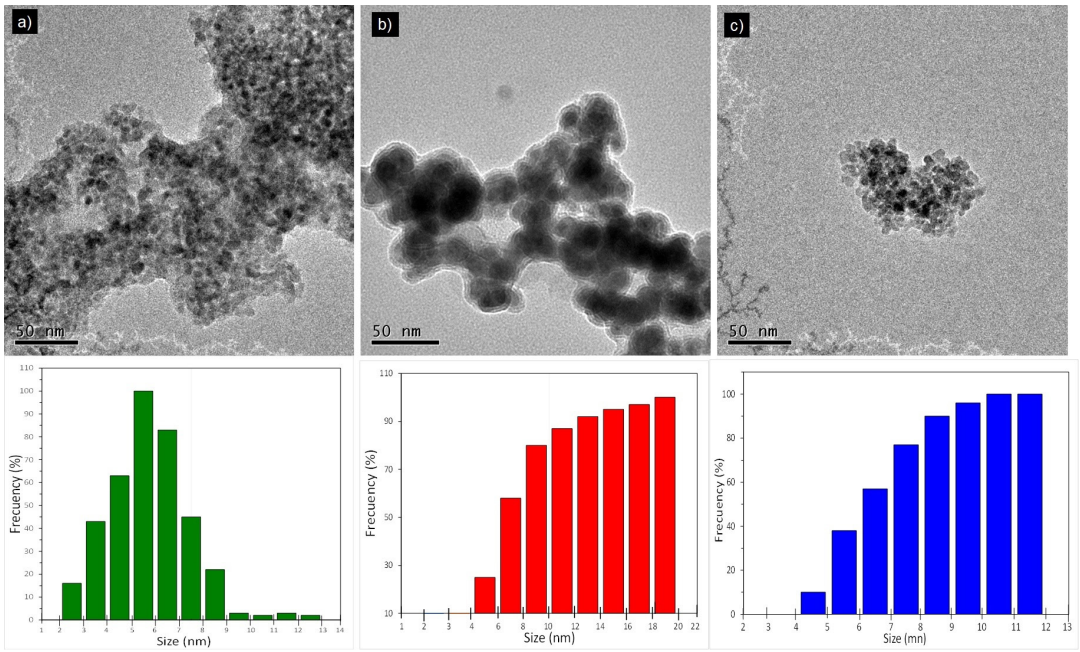

Fig. 9 TEM images (top) and size distribution histograms (bottom) of the FeCuNS. a) Fe:Cu 75:25 wt.%, b) Fe:Cu 50:50 wt.% and c) Fe:Cu 25:75 wt.%

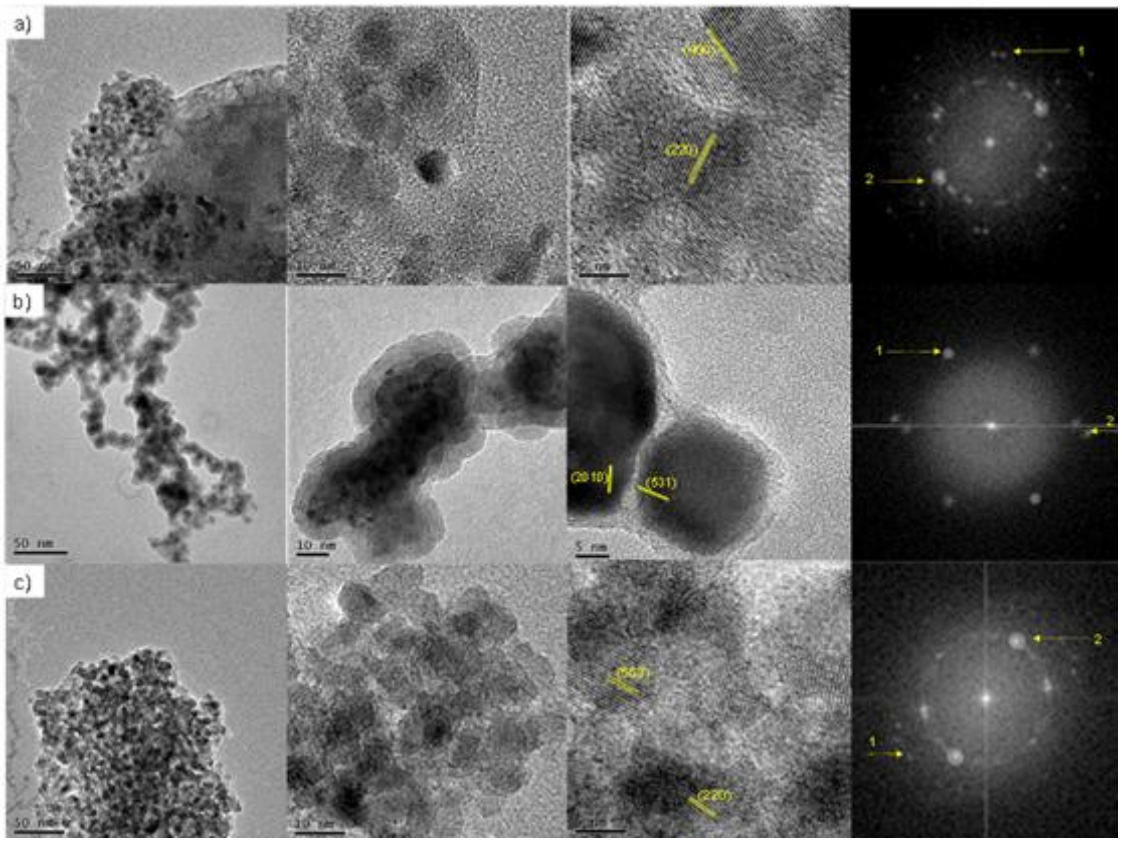

Fig. 10 HRTEM images of the FeCuNS. a) Fe:Cu 75:25 wt.%, b) Fe:Cu 50:50 wt.% and c) Fe:Cu 25:75 wt.%, with the corresponding FFT.

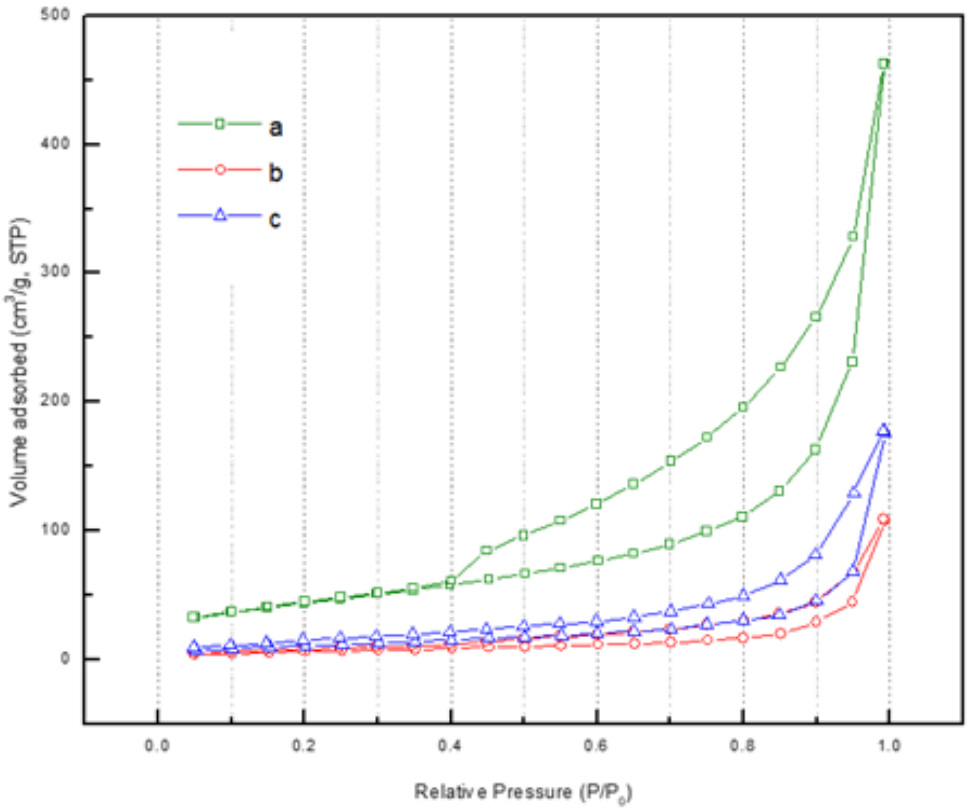

Fig. 11 N_2 adsorption/desorption isotherms of the FeCuNS. a) Fe:Cu 75:25 wt.%, b) Fe:Cu 50:50 wt.% and c) Fe:Cu 25:75 wt.%

Table 2 Textural properties of FeCuNS at different Fe and Cu wt.%.

FeCuNS (wt.%) sample	S_{BET}[a](m^2g^{-1})	V_{Total}[b](cm^3g^{-1})	D_{BJH}[c](nm)
75:25	158.169	0.2261	2.1168
50:50	47.940	0.3015	2.0390
25:75	40.971	0.2247	2.0485

[a]Specific surface areas. [b]Total pore volume. [c]Pore diameter.

Fig. 10c shows an interplanar distance of 2.063 nm, which can be indexed as the (220) plane associated with copper iron oxide ($CuFe_2O_4$). Furthermore, the SAED patterns confirm the presence of magnetite as the diffraction rings can be indexed based on the JCPDF No.79-0416 card.

N_2 adsorption–desorption isotherms of the FeCuNS samples are illustrated in Fig. 11. All samples exhibit typical III N_2 adsorption isotherms. Specifically, the inflections at P/P_0 = 0.4–0.6 reveal the narrow pore size distribution of mesoporous materials [20]. Table 2 shows the textural properties of Fe-Cu nanoparticles at the different metal ion concentrations used in the synthesis. The BET surface area increases in the 75:25 wt.% FeCuNS sample, while it decreases in 25:75 wt.% FeCuNS sample, which can be attributed to the saturation of nanostructures pores due, perhaps, to the increasing amount of Cu in the samples. However, this needs to be studied further.

CONCLUSIONS

FeCuNS were prepared in three different Fe:Cu ratios, namely 75:25, 50:50, and 25:75 wt. %, by an aqueous reduction process using $NaBH_4$, under N_2 atmosphere. The main phases in these nanostructures, as determined by XRD, were Fe_2O_3, Fe_3O_4 and $CuFe_2O_4$. The main peak obtained at $2\theta = 43.33°$ also revealed the formation of the nanoalloy Fe-Cu (JCPDS No.065-7002, as $FeCu_4$) in the 50:50 wt.% and 25:75 wt.% FeCuNS samples, which can be indexed as a face-centered cubic structure (FCC). According to the TEM results, the obtained FeCuNS tend to form agglomerates,

which can be associated to the magnetic nature of some metal oxides present in the nanomaterials, and, remarkably, their particle average size ranges from 6.5 to 11 nm. The XPS analysis of the FeCuNS further confirms the existence of $FeCu_4$ (Fe $2p_{3/2}$ at 706.7 eV), along with the presence of the other main iron and copper oxides phases.

ACKNOWELDGMENTS

The authors are thankful to Dr. Uvaldo Hernández Balderas, Dr. Gustavo López-Tellez, and L. I. A. María Citlalit Martínez Soto (CCIQS UAEM-UNAM) for X-ray powder diffraction analyses, XPS analyses and computing assistance, respectively. RZL thanks CONACyT for PhD scholarship (273831).

FUNDING

This work was funded by Universidad Autónoma del Estado de México.

CONFLICT OF INTEREST

The authors declare no conflict of interest.

REFERENCES

1. Maity D, Agrawal DC. Synthesis of iron oxide nanoparticles under oxidizing environment and their stabilization in aqueous and non-aqueous media. Journal of Magnetism and Magnetic Materials. 2007;308(1):46-55. https://doi.org/10.1016/j.jmmm.2006.05.001
2. Wu W, He Q, Jiang C. Magnetic Iron Oxide Nanoparticles: Synthesis and Surface Functionalization Strategies. Nanoscale Research Letters. 2008;3(11):397. https://doi.org/10.1007/s11671-008-9174-9
3. Gawande MB, Goswami A, Felpin F-X, Asefa T, Huang X, Silva R, et al. Cu and Cu-Based Nanoparticles: Synthesis and Applications in Catalysis. Chemical Reviews. 2016;116(6):3722-811. https://doi.org/10.1021/acs.chemrev.5b00482
4. Hokita Y, Kanzaki M, Sugiyama T, Arakawa R, Kawasaki H. High-Concentration Synthesis of Sub-10-nm Copper Nanoparticles for Application to Conductive Nanoinks. ACS Applied Materials & Interfaces. 2015;7(34):19382-9. https://doi.org/10.1021/acsami.5b05542
5. Wilson NH, Ragothaman M, Palanisamy T. Bimetallic Copper-Iron Oxide Nanoparticle-Coated Leathers for Lighting Applications. ACS Applied Nano Materials. 2021;4(4):4055-69. https://doi.org/10.1021/acsanm.1c00388
6. Manickam-Periyaraman P, Espinosa JC, Ferrer B, Subramanian S, Álvaro M, García H, et al. Bimetallic iron-copper oxide nanoparticles supported on nanometric diamond as efficient and stable sunlight-assisted Fenton photocatalyst. Chemical Engineering Journal. 2020;393:124770. https://doi.org/10.1016/j.cej.2020.124770
7. Zhang P, Hou D, O'Connor D, Li X, Pehkonen S, Varma RS, et al. Green and Size-Specific Synthesis of Stable Fe-Cu Oxides as Earth-Abundant Adsorbents for Malachite Green Removal. ACS Sustainable Chemistry & Engineering. 2018;6(7):9229-36. https://doi.org/10.1021/acssuschemeng.8b01547
8. Cahn RW. Intermetallics: New physics. Contemporary Physics. 2001;42(6):365-75. https://doi.org/10.1080/00107510110084084
9. O'Carroll D, Sleep B, Krol M, Boparai H, Kocur C. Nanoscale zero valent iron and bimetallic particles for contaminated site remediation. Advances in Water Resources. 2013;51:104-22. https://doi.org/10.1016/j.advwatres.2012.02.005
10. Huang J, Kunitake T. Nano-Precision Replication of Natural Cellulosic Substances by Metal Oxides. Journal of the American Chemical Society. 2003;125(39):11834-5. https://doi.org/10.1021/ja037419k
11. Kamat PV. Photophysical, Photochemical and Photocatalytic Aspects of Metal Nanoparticles. The Journal of Physical Chemistry B. 2002;106(32):7729-44. https://doi.org/10.1021/jp0209289
12. Sun S, Murray CB, Weller D, Folks L, Moser A. Monodisperse FePt nanoparticles and ferromagnetic FePt nanocrystal superlattices. Science. 2000;287(5460):1989-92. https://doi.org/10.1126/science.287.5460.1989
13. Agarwal S, Al-Abed SR, Dionysiou DD. Enhanced Corrosion-Based Pd/Mg Bimetallic Systems for Dechlorination of PCBs. Environmental Science & Technology. 2007;41(10):3722-7. https://doi.org/10.1021/es062886y
14. Yen CH, Shimizu K, Lin Y-Y, Bailey F, Cheng IF, Wai CM. Chemical Fluid Deposition of Pt-Based Bimetallic Nanoparticles on Multiwalled Carbon Nanotubes for Direct Methanol Fuel Cell Application. Energy & Fuels. 2007;21(4):2268-71. https://doi.org/10.1021/ef0606409
15. Bransfield SJ, Cwiertny DM, Roberts AL, Fairbrother DH. Influence of Copper Loading and Surface Coverage on the Reactivity of Granular Iron toward 1,1,1-Trichloroethane. Environmental Science & Technology. 2006;40(5):1485-90. https://doi.org/10.1021/es051300p
16. Link S, El-Sayed MA. Size and Temperature Dependence of the Plasmon Absorption of Colloidal Gold Nanoparticles. The Journal of Physical Chemistry B. 1999;103(21):4212-7. https://doi.org/10.1021/jp984796o
17. Tzitzios V, Niarchos D, Gjoka M, Boukos N, Petridis D. Synthesis and Characterization of 3D CoPt Nanostructures. Journal of the American Chemical Society. 2005;127(40):13756-7. https://doi.org/10.1021/ja053044m
18. Cheng ZH, Gao L, Deng ZT, Liu Q, Jiang N, Lin X, et al. Epitaxial Growth of Iron Phthalocyanine at the Initial Stage on Au(111) Surface. The Journal of Physical Chemistry C. 2007;111(6):2656-60. https://doi.org/10.1021/jp0660738
19. Govorov AO, Richardson HH. Generating heat with metal nanoparticles. Nano Today. 2007;2(1):30-8. https://doi.org/10.1016/S1748-0132(07)70017-8
20. Wang J, Liu C, Hussain I, Li C, Li J, Sun X, et al. Iron-copper bimetallic nanoparticles supported on hollow mesoporous silica spheres: the effect of Fe/Cu ratio on heterogeneous Fenton degradation of a dye. RSC Advances. 2016;6(59):54623-35. https://doi.org/10.1039/C6RA08501F
21. Timofeeva MN, Khankhasaeva ST, Talsi EP, Panchenko VN, Golovin AV, Dashinamzhilova ET, et al. The effect of Fe/Cu ratio in the synthesis of mixed Fe,Cu,Al-

clays used as catalysts in phenol peroxide oxidation. Applied Catalysis B: Environmental. 2009;90(3):618-27. https://doi.org/10.1016/j.apcatb.2009.04.024
22. Han Z, Dong Y, Dong S. Copper-iron bimetal modified PAN fiber complexes as novel heterogeneous Fenton catalysts for degradation of organic dye under visible light irradiation. Journal of Hazardous Materials. 2011;189(1):241-8. https://doi.org/10.1016/j.jhazmat.2011.02.026
23. Rossi AF, Martins RC, Quinta-Ferreira RM. Composition Effect of Iron-Copper Composite Catalysts in the Fenton Heterogeneous Process Efficiency and Cooxidation Synergy Assessment. Industrial & Engineering Chemistry Research. 2014;53(40):15369-73. https://doi.org/10.1021/ie501193x
24. Trujillo-Reyes J, Sánchez-Mendieta V, José Solache-Ríos M, Colín-Cruz A. Removal of remazol yellow from aqueous solution using Fe-Cu and Fe-Ni nanoscale oxides and their carbonaceous composites. Environmental Technology. 2012;33(5):545-54. https://doi.org/10.1080/09593330.2011.584571
25. Huber DL. Synthesis, properties, and applications of iron nanoparticles. Small. 2005;1(5):482-501. https://doi.org/10.1002/smll.200500006
26. Basu S, Chakravorty D. Optical properties of nanocomposites with iron core-iron oxide shell structure. Journal of non-crystalline solids. 2006;352(5):380-5. https://doi.org/10.1016/j.jnoncrysol.2006.01.006
27. Yang C, Wu J, Hou Y. Fe3O4 nanostructures: synthesis, growth mechanism, properties and applications. Chemical Communications. 2011;47(18):5130-41. https://doi.org/10.1039/c0cc05862a
28. Xue W, Fang K, Qiu H, Li J, Mao W. Electrical and magnetic properties of the Fe3O4-polyaniline nanocomposite pellets containing DBSA-doped polyaniline and HCl-doped polyaniline with Fe3O4 nanoparticles. Synthetic Metals. 2006;156(7):506-9. https://doi.org/10.1016/j.synthmet.2005.06.021
29. Guo L, Huang Q-J, Li X-Y, Yang S. PVP-Coated Iron Nanocrystals: Anhydrous Synthesis, Characterization, and Electrocatalysis for Two Species. Langmuir. 2006;22(18):7867-72. https://doi.org/10.1021/la060975i
30. Galdames A, Ruiz-Rubio L, Orueta M, Sánchez-Arzalluz M, Vilas-Vilela JL. Zero-Valent Iron Nanoparticles for Soil and Groundwater Remediation. International Journal of Environmental Research and Public Health [Internet]. 2020; 17(16). https://doi.org/10.3390/ijerph17165817
31. Tanabe K. Optical radiation efficiencies of metal nanoparticles for optoelectronic applications. Materials Letters. 2007;61(23):4573-5. https://doi.org/10.1016/j.matlet.2007.02.053
32. Garitaonandia JS, Insausti M, Goikolea E, Suzuki M, Cashion JD, Kawamura N, et al. Chemically Induced Permanent Magnetism in Au, Ag, and Cu Nanoparticles: Localization of the Magnetism by Element Selective Techniques. Nano Letters. 2008;8(2):661-7. https://doi.org/10.1021/nl073129g
33. You T, Niwa O, Tomita M, Ando H, Suzuki M, Hirono S. Characterization and electrochemical properties of highly dispersed copper oxide/hydroxide nanoparticles in graphite-like carbon films prepared by RF sputtering method. Electrochemistry Communications. 2002;4(5):468-71. https://doi.org/10.1016/S1388-2481(02)00340-5
34. Haq S, Carew A, Raval R. Nitric oxide reduction by Cu nanoclusters supported on thin Al2O3 films. Journal of Catalysis. 2004;221(1):204-12. https://doi.org/10.1016/S0021-9517(03)00311-7
35. de Sousa PVF, de Oliveira AF, da Silva AA, Lopes RP. Environmental remediation processes by zero valence copper: reaction mechanisms. Environmental Science and Pollution Research. 2019;26(15):14883-903. https://doi.org/10.1007/s11356-019-04989-3
36. Longano D, Ditaranto N, Sabbatini L, Torsi L, Cioffi N. Synthesis and Antimicrobial Activity of Copper Nanomaterials. In: Cioffi N, Rai M, editors. Nano-Antimicrobials: Progress and Prospects. Berlin, Heidelberg: Springer Berlin Heidelberg; 2012. p. 85-117. https://doi.org/10.1007/978-3-642-24428-5_3
37. Freeman RG, Hommer MB, Grabar KC, Jackson MA, Natan MJ. Ag-Clad Au Nanoparticles: Novel Aggregation, Optical, and Surface-Enhanced Raman Scattering Properties. The Journal of Physical Chemistry. 1996;100(2):718-24. https://doi.org/10.1021/jp951379s
38. Srinoi P, Chen Y-T, Vittur V, Marquez MD, Lee TR. Bimetallic Nanoparticles: Enhanced Magnetic and Optical Properties for Emerging Biological Applications. Applied Sciences [Internet]. 2018; 8(7). https://doi.org/10.3390/app8071106
39. Liz-Marzan LM, Philipse AP. Stable hydrosols of metallic and bimetallic nanoparticles immobilized on imogolite fibers. The Journal of Physical Chemistry. 1995;99(41):15120-8. https://doi.org/10.1021/j100041a031
40. Esumi K, Shiratori M, Ishizuka H, Tano T, Torigoe K, Meguro K. Preparation of bimetallic palladium-platinum colloids in organic solvent by solvent extraction-reduction. Langmuir. 1991;7(3):457-9. https://doi.org/10.1021/la00051a007
41. Dhas NA, Raj CP, Gedanken A. Synthesis, Characterization, and Properties of Metallic Copper Nanoparticles. Chemistry of Materials. 1998;10(5):1446-52. https://doi.org/10.1021/cm9708269
42. Mizukoshi Y, Okitsu K, Maeda Y, Yamamoto TA, Oshima R, Nagata Y. Sonochemical Preparation of Bimetallic Nanoparticles of Gold/Palladium in Aqueous Solution. The Journal of Physical Chemistry B. 1997;101(36):7033-7. https://doi.org/10.1021/jp9638090
43. Remita S, Mostafavi M, Delcourt MO. Bimetallic Ag-Pt and Au-Pt aggregates synthesized by radiolysis. Radiation Physics and Chemistry. 1996;47(2):275-9. https://doi.org/10.1016/0969-806X(94)00172-G
44. Sato T, Kuroda S, Takami A, Yonezawa Y, Hada H. Photochemical formation of silver-gold (Ag-Au) composite colloids in solutions containing sodium alginate. Applied organometallic chemistry. 1991;5(4):261-8. https://doi.org/10.1002/aoc.590050409
45. Mulvaney P, Giersig M, Henglein A. Electrochemistry of multilayer colloids: preparation and absorption spectrum of gold-coated silver particles. The Journal of Physical Chemistry. 1993;97(27):7061-4. https://doi.org/10.1021/j100129a022
46. Treguer M, de Cointet C, Remita H, Khatouri J, Mostafavi M, Amblard J, et al. Dose Rate Effects on Radiolytic Synthesis of Gold–Silver Bimetallic Clusters in Solution. The Journal of Physical Chemistry B. 1998;102(22):4310-21. https://doi.org/10.1021/jp981467n

47. Hodak JH, Henglein A, Giersig M, Hartland GV. Laser-Induced Inter-Diffusion in AuAg Core–Shell Nanoparticles. The Journal of Physical Chemistry B. 2000;104(49):11708-18. https://doi.org/10.1021/jp002438r
48. Chen Y-H, Yeh C-S. A new approach for the formation of alloy nanoparticles: laser synthesis of gold-silver alloy from gold-silver colloidal mixtures. Chemical Communications. 2001(4):371-2. https://doi.org/10.1039/b009854j
49. Slocik JM, Naik RR. Biologically programmed synthesis of bimetallic nanostructures. Advanced Materials. 2006;18(15):1988-92. https://doi.org/10.1002/adma.200600327
50. Zhang G, Ren Z, Zhang X, Chen J. Nanostructured iron(III)-copper(II) binary oxide: A novel adsorbent for enhanced arsenic removal from aqueous solutions. Water Research. 2013;47(12):4022-31. https://doi.org/10.1016/j.watres.2012.11.059
51. Zhu N, Luan H, Yuan S, Chen J, Wu X, Wang L. Effective dechlorination of HCB by nanoscale Cu/Fe particles. Journal of Hazardous Materials. 2010;176(1):1101-5. https://doi.org/10.1016/j.jhazmat.2009.11.092
52. Sepúlveda P, Rubio MA, Baltazar SE, Rojas-Nunez J, Sánchez Llamazares JL, Garcia AG, et al. As(V) removal capacity of FeCu bimetallic nanoparticles in aqueous solutions: The influence of Cu content and morphologic changes in bimetallic nanoparticles. Journal of Colloid and Interface Science. 2018;524:177-87. https://doi.org/10.1016/j.jcis.2018.03.113
53. Qiao Y, Ni Y, Kong F, Li R, Zhang C, Kong A, et al. Pyrolytic Carbon- coated Cu- Fe Alloy Nanoparticles with High Catalytic Performance for Oxygen Electroreduction. Chemistry-An Asian Journal. 2019;14(15):2676-84. https://doi.org/10.1002/asia.201900524
54. Wei ZS, Zeng GH, Xie ZR, Ma CY, Liu XH, Sun JL, et al. Microwave catalytic NOx and SO2 removal using FeCu/zeolite as catalyst. Fuel. 2011;90(4):1599-603. https://doi.org/10.1016/j.fuel.2010.11.021
55. Yi H, Zhao S, Tang X, Song C, Gao F, Zhang B, et al. Low-temperature hydrolysis of carbon disulfide using the FeCu/AC catalyst modified by non-thermal plasma. Fuel. 2014;128:268-73. https://doi.org/10.1016/j.fuel.2014.03.021
56. Dlamini NG, Basson AK, Pullabhotla VS. Synthesis and Application of FeCu Bimetallic Nanoparticles in Coal Mine Wastewater Treatment. Minerals [Internet]. 2021; 11(2). https://doi.org/10.3390/min11020132